Applied Physics Express

LETTER • **OPEN ACCESS**

Continuous-wave lasing of AlGaN-based ultraviolet laser diode at 274.8 nm by current injection

To cite this article: Ziyi Zhang *et al* 2022 *Appl. Phys. Express* **15** 041007

OPEN ACCESS

Applied Physics Express 15, 041007 (2022) LETTER

https://doi.org/10.35848/1882-0786/ac6198

Continuous-wave lasing of AlGaN-based ultraviolet laser diode at 274.8 nm by current injection

Ziyi Zhang[1,2*], Maki Kushimoto[3], Akira Yoshikawa[1,2], Koji Aoto[2], Leo J. Schowalter[2], Chiaki Sasaoka[2], and Hiroshi Amano[2]

[1]Innovative Devices R&D Center, Corporate Research & Development, Asahi Kasei Corporation, Chiyoda, Tokyo 100-0006, Japan
[2]Center for Integrated Research of Future Electronics, Institute of Materials Research and System for Sustainability, Nagoya University, Chikusa, Aichi 464-8601, Japan
[3]Graduate School of Engineering, Nagoya University, Chikusa, Aichi 464-8603, Japan

*E-mail: zhang.zc@om.asahi-kasei.co.jp

Received March 10, 2022; revised March 19, 2022; accepted March 28, 2022; published online April 6, 2022

We demonstrated continuous-wave lasing of an AlGaN-based ultraviolet laser diode, fabricated on a single-crystal AlN substrate when operating at 5 °C. The threshold current density and device series resistance were reduced by improvements to the epitaxial structure and electrode arrangement. A peak wavelength of 274.8 nm was observed for lasing at a drive current over 110 mA, which corresponded to a threshold current density of 3.7 kA cm^{-2}. The operating voltage at the threshold current was as low as 9.6 V. © 2022 The Author(s). Published on behalf of The Japan Society of Applied Physics by IOP Publishing Ltd

Laser diodes (LDs) in the ultraviolet C band (200–280 nm, UVC), based on AlGaN, are expected to be used as a low-cost, environmentally friendly, and efficient new laser light source for various applications, including bio-/chemical sensing, particle detection, rapid sterilization, solar-blind communication, and material processing. However, there are several challenges to realizing AlGaN-based UVC LDs, such as difficulty in epitaxial growth of high-quality AlGaN active layers on foreign substrates,[1)] insufficient carrier injection capability due to the poor activation of Mg-doped AlGaN[2–4)] and high operating voltage due to the wide bandgap of AlGaN. However, recent research provides key technologies to address these issues. Active layers formed on free-standing AlN single-crystal substrates[5,6)] were demonstrated to achieve high internal quantum efficiencies[7)] and low lasing threshold powers by optical pumping measurements.[8–13)] Polarization-induced doping techniques,[14,15)] which can provide p-type conductivity in wide-bandgap nitrides, have been demonstrated to be applicable to AlGaN films that are sufficiently thick so as to be used as p-type cladding layers in LDs.[16,17)] Moreover, it was demonstrated that p-type conductivity can be achieved even without any impurity doping using this approach.[18–20)] As a result, the low internal loss was achievable.[21)] Although these technologies led to breakthroughs in the realization of AlGaN-based LDs in UVC regions during pulsed current operation,[22,23)] the threshold current densities were still relatively high (10 kA cm^{-2} level) compared to blue laser diodes and continuous-wave (CW) lasing was not achieved. In this work, the required threshold gain was further reduced by improving the optical confinement and the threshold current density was improved while the drive voltage was reduced. As a result, CW lasing at 5 °C was successfully demonstrated for the first time.

One way to reduce the threshold current density is by reducing the gain required to initiate lasing; so-called the threshold gain $g_{th} = (\alpha_i + \alpha_m)/\Gamma_{QW}$. A reduction of the internal loss α_i and the mirror loss α_m has already been achieved by employing a p-type distributed polarization doping without any impurities and by utilizing a high-reflectivity coating on cavity facets,[21,24)] respectively. In the current work, the quantum well optical confinement factor (Γ_{QW}) was optimized through structural modifications to further reduce g_{th}. The LD structures were epitaxially grown on the Al-face of single-crystal AlN substrates by metal organic chemical vapor deposition. The reference structure (referred to here as Device A), consists of a 350 nm n-type Si-doped $Al_{0.7}Ga_{0.3}N$ cladding layer, a 100 nm $Al_{0.63}Ga_{0.37}N$ waveguide with two 4.5 nm quantum well active layers, a 320 nm p-type distributed polarization doped cladding layer (p-DPD), and a p-type contact layer including an additional Al compositional grading layer and a Mg-doped GaN. The Al composition x of $Al_xGa_{1-x}N$ was decreased from 1.0 to 0.7 in the growth direction of the p-DPD without any intentional impurity doping. The device was fabricated by, first exposing the n-type cladding layer by dry etching and then etching a stripe in the p-contact layer with a width of 5 μm in the ⟨1–100⟩ direction for further current narrowing (mesa stripe formation). SiO_2 was deposited as a passivation layer which was, then followed by the formation of V/Al/Ni/Au-based n-electrode beside the mesa stripe on the exposed n-type cladding and a Ni/Au-based p-electrode on the p-type contact layer of the mesa stripe. The fabricated wafers were then thinned down to 100 μm and cleaved along the ⟨11–20⟩ direction to form a 600 μm long cavity with atomically flat (1–100) facets at either end. This was followed by depositing 5 pairs of HfO_2/SiO_2 high-reflectivity coatings (90%) on both cleaved facets.

The fundamental TE mode of the reference structure (Device A) was calculated using the measured refractive indexes[21)] as shown in Fig. 1(a) and Γ_{QW} was determined to be 4%. Another prototype structure, Device B, was designed to increase the confinement factor as shown in Fig. 1(b). Here an n-type $Al_{0.75}Ga_{0.25}N$ cladding layer with a lower refractive index was used to better confine modes that leak out to the n-type cladding layer, while the thickness of the waveguide layer was increased to 120 nm. In addition, the position of the quantum wells was adjusted to the peak position of the mode. In this Device B structure, the Γ_{QW} was modeled to be 6%. This improvement was designed so that all AlGaN layers could be grown pseudomorphically on the AlN substrate, which was then confirmed by X-ray reciprocal space

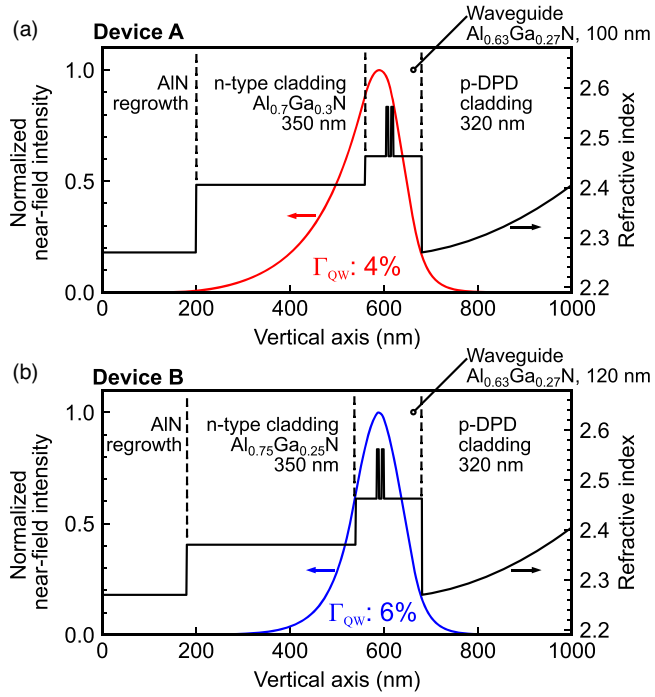

Fig. 1. (Color online) Refractive index profiles and normalized near-field intensity of fundamental TE mode of (a) Device A and (b) Device B.

mapping of the (11–24) plane after actual epitaxial growth of the Device B structure.

The light–current–voltage (L–I–V) characteristics of the fabricated Devices A and B were measured at room temperature and with a pulse width (repetition rate) of 100 ns (2 kHz), corresponding to a duty cycle of 0.02%. The resulting edge emission power was measured using a calibrated photon multimeter. Figure 2 shows the L–I–V characteristics of Devices A and B under pulsed current operation. The I_{th} was reduced from 325 mA (11 kA cm^{-2}) to 210 mA (7 kA cm^{-2}) where the current density is calculated by assuming that the current flow is limited to the region of the p-electrode. Since the slope efficiency was maintained at 0.035 W A^{-1} for both Devices, the reduction of I_{th} in Device

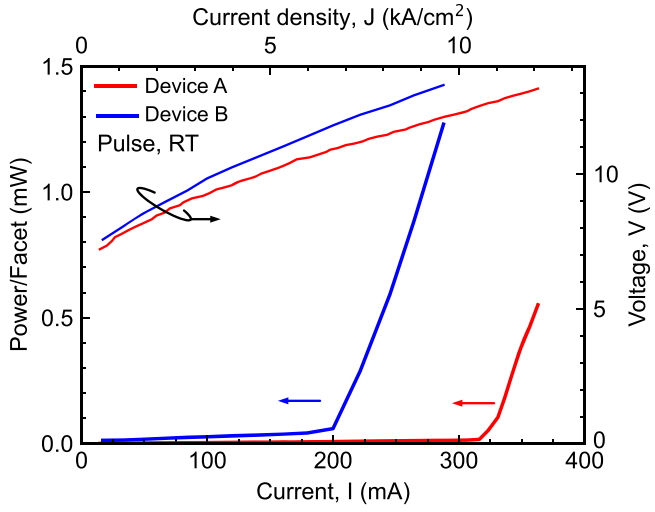

Fig. 2. (Color online) L–I–V characteristics of Devices A and B with different light confinement factors (Γ_{QW}) measured under pulsed current operation (a pulse width of 100 ns and a duty cycle of 0.02%) at room temperature.

B has to be a result of the larger confinement factor, which reduced g_{th}. On the other hand, the series resistance (R_s) of Device B increased to 19 Ω from 14 Ω measured for Device A. This R_s increase for Device B is likely due to the higher Al composition x for the n-type $Al_xGa_{1-x}N$ cladding layer. Indeed, the resistivity of the n-type cladding increased from 0.008 Ω cm ($x = 0.7$) to 0.011 Ω cm ($x = 0.75$), as shown by the eddy current sheet resistance measurement, which reasonably explains the increase in R_s since 60% of device resistance is accounted for by current transport through this layer.

Next, a double-sided arrangement of n-electrodes was also employed to lower R_s as shown in Fig. 3(a). New Devices C and D were fabricated: where the only difference between them was that Device C had a single n-electrode placed beside the mesa stripe (similar to Devices A and B) whereas Device D had a set of n-electrodes placed on both sides of the mesa stripe to decrease the lateral path resistance of the n-type cladding layer (referred to as a "double-sided arrangement"). The epitaxial growth conditions for both devices were also modified to reduce threshold current density by improving the internal quantum efficiency. It has been a common issue that high Al content $Al_xGa_{1-x}N$ often seems to have higher densities of point defects and these defects may serve as nonradiative recombination centers for light-emitting devices resulting in the loss of carriers.[25,26] Therefore, based on the idea of reducing point defects by controlling surface supersaturation,[7,12,27] the epitaxial growth conditions were systematically modified to achieve stronger EL emission intensity while using the Device B structure. Devices C and D were both packaged in TO-Can including wire bonding so that current injection from both n-electrodes of Device D was accomplished. The L–I characteristics were then measured under pulsed current operation (a pulse width of 100 ns and a duty cycle of 0.02%) at room temperature, as shown in Fig. 3(b).

Devices C and D were confirmed to have the same I_{th} of 85 mA (2.8 kA cm^2) and a slope efficiency of 0.12 W A^{-1}. The reduction in I_{th} for both Devices C and D, when compared

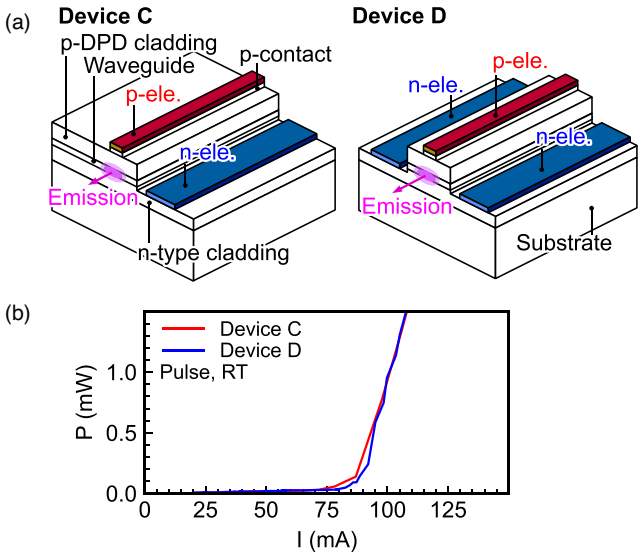

Fig. 3. (Color online) (a) Double-sided n-electrode arrangement in Device D compared with the referenced arrangement of Device C (similar to Devices A and B) to reduce series resistance. (b) Comparison of the L–I characteristics of Devices C and D under pulsed current operation (a pulse width of 100 ns and a duty cycle of 0.02%) at room temperature.

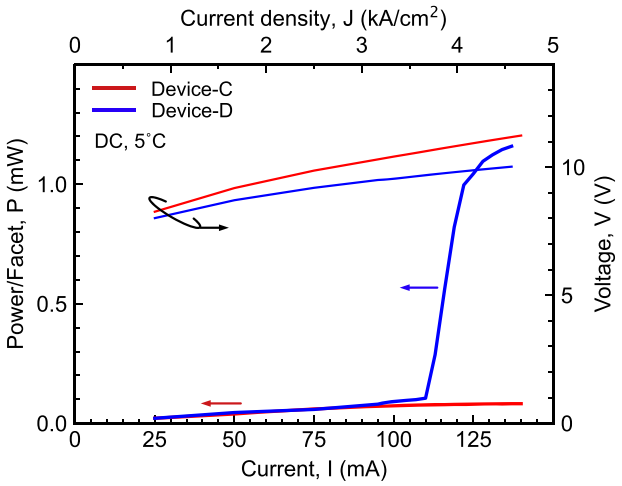

Fig. 4. (Color online) *L–I–V* characteristics of packaged Devices C and D with DC current sweep when heat sink temperature maintained at 5 °C.

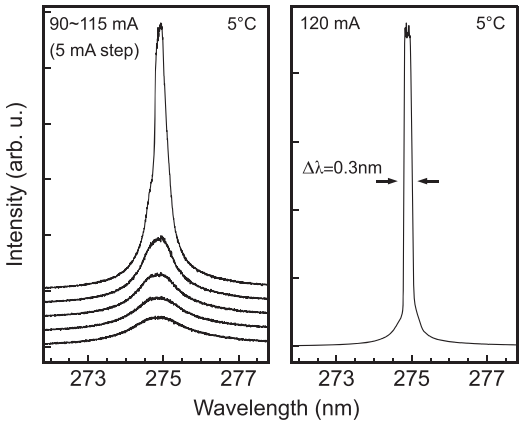

Fig. 5. Measured optical spectra of packaged Device D with heat sink temperature maintained at 5 °C.

to Device B, indicates that an increase in internal quantum efficiency was realized by modifying the epitaxial growth conditions as discussed above. The increase of slope efficiency indicates that the injection efficiency was also improved by roughly a factor of 3. Direct current (DC) *L–I–V* measurements were performed while the packaged Devices C and D were connected to a heat sink maintained at 5 °C with a Peltier cooler. A photodetector was used to measure edge emission power while a DC sweep was performed at drive currents from 25 mA to 135 mA in 3 s. Figure 4 shows the *L–I–V* characteristics of Devices C and D under DC operation. R_s for Device D, with a double-sided n-electrode arrangement, was reduced to 12 Ω as opposed to 20 Ω for Device C. Lasing was observed with CW operation at currents over 110 mA for Device D, which corresponds to a threshold current density of 3.7 kA cm^{-2}. The operating voltage at I_{th} was 9.6 V. On the other hand, CW lasing was not observed for Device C even at drive currents up to 140 mA.

Edge emission spectra were measured for Device D at a drive current around the I_{th}. To prevent thermal effects on the Device during spectral imaging, measurements were carried out with a pulse width (repetition rate) of 10 ms (1 Hz), corresponding to a duty cycle of 1%. Figure 5 shows the spectra of edge emission as the drive current was increased from 90 mA to 120 mA by 5 mA steps. A clear, narrow peak at 274.8 nm emerged above I_{th} with a spectral width $\Delta\lambda$ of 0.3 nm. The longitudinal mode could not clearly be resolved as its expected free spectrum range of 0.026 nm is comparable to the 0.005 nm minimum resolution of the spectrometer.

The DC *L–I* curve of Device D lost linearity at drive currents above 120 mA (input power 1.2 W), but no such output saturation was observed under the pulsed current operation, suggesting the possibility of output saturation was due to heat generation. The fact that Device C, with higher operating voltage (due to higher R_s), could not achieve CW lasing emphasizes the importance of reducing the required threshold input power and the need for good thermal management in these devices. Therefore, the future focus will still be on reducing the threshold current density and series resistance. The threshold current density should be further reduced by increasing the internal quantum efficiency and injection efficiency. Although results suggest the injection efficiency was increased for Devices C and D, it is still expected to be <10% which is still much lower than that of InGaN-based laser diodes, which are typically reported to be 60% or more at their operating current density.[28,29] To reduce series resistance, there are several challenges that need to be addressed such as the thickness limitation of the n-type cladding to avoid crystal relaxation (which would create threading dislocations), the fact that the n- and p-electrodes must be placed side by side on the epitaxial side of the wafer owing to the lack of an n-type substrate[30,31] and the limitation of p-electrode placement due to defect formation seen in the mesa stripes[32] which forces electron transport to be over larger distances.

In summary, we have demonstrated CW lasing of an AlGaN based UVC laser diode under direct current operation at 5 °C. Lasing was observed at a CW operation drive current above 110 mA (3.7 kA cm^{-2} current density) with an emission wavelength of 274.8 nm. A lower threshold current was achieved by reducing the threshold gain through improving the optical confinement factor and by improving the epitaxial growth condition. Furthermore, the operating voltage was decreased through the use of a double-sided n-electrode arrangement. The results reported here are promising for the realization of a practical UVC LD. However, a reduction of the minimum operating power is required by reducing the threshold current density and the series resistance of the device still further.

Acknowledgments The authors would like to thank Professor Yoshio Honda of Nagoya University and Dr. Masato Toita, Mr. Kazuhiro Nagase, and Dr. Naohiro Kuze of Asahi Kasei Corporation for their invaluable discussion and considerable support. The authors would also like to thank Dr. Katsunori Nishii and working members of C-TEFs of Nagoya University for their great contribution to the development of the laser diode process. This work was supported by KAKENHI (21H04560).

ORCID iDs Ziyi Zhang https://orcid.org/0000-0001-9617-9049 Maki Kushimoto https://orcid.org/0000-0003-3974-7139 Leo J. Schowalter https://orcid.org/0000-0002-4854-8521

1) K. Ban, J. Yamamoto, K. Takeda, K. Ide, M. Iwaya, T. Takeuchi, S. Kamiyama, I. Akasaki, and H. Amano, Appl. Phys. Express **4**, 052101 (2011).
2) M. Katsuragawa, S. Sota, M. Komori, C. Anbe, T. Takeuchi, H. Sakai, H. Amano, and I. Akasaki, J. Cryst. Growth **189–190**, 528 (1998).
3) M. L. Nakarmi, N. Nepal, J. Y. Lin, and H. X. Jiang, Appl. Phys. Lett. **94**, 091903 (2009).
4) T. Kinoshita, T. Obata, T. Nagashima, H. Yanagi, B. Moody, S. Mita, S. i. Inoue, Y. Kumagai, A. Koukitu, and Z. Sitar, Appl. Phys. Express **6**, 092103 (2013).

5) R. T. Bondokov, S. G. Mueller, K. E. Morgan, G. A. Slack, S. Schujman, M. C. Wood, J. A. Smart, and L. J. Schowalter, J. Cryst. Growth **310**, 4020 (2008).
6) S. G. Mueller, R. T. Bondokov, K. E. Morgan, G. A. Slack, S. B. Schujman, J. Grandusky, J. A. Smart, and L. J. Schowalter, Phys. Status Solidi A **206**, 1153 (2009).
7) Z. Bryan, I. Bryan, J. Xie, S. Mita, Z. Sitar, and R. Collazo, Appl. Phys. Lett. **106**, 142107 (2015).
8) T. Wunderer, C. L. Chua, Z. Yang, J. E. Northrup, N. M. Johnson, G. A. Garrett, H. Shen, and M. Wraback, Appl. Phys. Express **4**, 092101 (2011).
9) Z. Lochner et al., Appl. Phys. Lett. **102**, 101110 (2013).
10) M. Martens et al., IEEE Photonics Technol. Lett. **26**, 342 (2014).
11) W. Guo et al., J. Appl. Phys. **115**, 103108 (2014).
12) R. Kirste, Q. Guo, J. H. Dycus, A. Franke, S. Mita, B. Sarkar, P. Reddy, J. M. LeBeau, R. Collazo, and Z. Sitar, Appl. Phys. Express **11**, 082101 (2018).
13) Q. Guo et al., J. Appl. Phys. **126**, 223101 (2019).
14) D. Jena et al., Appl. Phys. Lett. **81**, 4395 (2002).
15) J. Simon, V. Protasenko, C. Lian, H. Xing, and D. Jena, Science **327**, 60 (2010).
16) R. Dalmau and B. Moody, ECS Trans. **86**, 31 (2018).
17) K. Sato, S. Yasue, Y. Ogino, S. Tanaka, M. Iwaya, T. Takeuchi, S. Kamiyama, and I. Akasaki, Appl. Phys. Lett. **114**, 191103 (2019).
18) S. Li, M. Ware, J. Wu, P. Minor, Z. Wang, Z. Wu, Y. Jiang, and G. J. Salamo, Appl. Phys. Lett. **101**, 122103 (2012).
19) Z. Zhang, M. Kushimoto, M. Horita, N. Sugiyama, L. J. Schowalter, C. Sasaoka, and H. Amano, Appl. Phys. Lett. **117**, 152104 (2020).
20) K. Sato et al., Appl. Phys. Express **14**, 096503 (2021).
21) Z. Zhang, M. Kushimoto, T. Sakai, N. Sugiyama, L. J. Schowalter, C. Sasaoka, and H. Amano, Jpn. J. Appl. Phys. **59**, 094001 (2020).
22) Z. Zhang, M. Kushimoto, T. Sakai, N. Sugiyama, L. J. Schowalter, C. Sasaoka, and H. Amano, Appl. Phys. Express **12**, 124003 (2019).
23) T. Sakai, M. Kushimoto, Z. Zhang, N. Sugiyama, L. J. Schowalter, Y. Honda, C. Sasaoka, and H. Amano, Appl. Phys. Lett. **116**, 122101 (2020).
24) T. T. Kao et al., Appl. Phys. Lett. **103**, 211103 (2013).
25) K. B. Nam, M. L. Nakarmi, J. Y. Lin, and H. X. Jiang, Appl. Phys. Lett. **86**, 222108 (2005).
26) T. A. Henry, A. Armstrong, A. A. Allerman, and M. H. Crawford, Appl. Phys. Lett. **100**, 043509 (2012).
27) S. Washiyama, P. Reddy, F. Kaess, R. Kirste, S. Mita, R. Collazo, and Z. Sitar, J. Appl. Phys. **124**, 115304 (2018).
28) H. Y. Ryu et al., Appl. Phys. Lett. **93**, 011105 (2008).
29) R. M. Farrell, D. A. Haeger, P. S. Hsu, K. Fujito, D. F. Feezell, S. P. DenBaars, J. S. Speck, and S. Nakamura, Appl. Phys. Lett. **99**, 171115 (2011).
30) R. Collazo, S. Mita, J. Xie, A. Rice, J. Tweedie, R. Dalmau, and Z. Sitar, Phys. Status Solidi C **8**, 2031 (2011).
31) J. S. Harris, J. N. Baker, B. E. Gaddy, I. Bryan, Z. Bryan, K. J. Mirrielees, P. Reddy, R. Collazo, Z. Sitar, and D. L. Irving, Appl. Phys. Lett. **112**, 152101 (2018).
32) M. Kushimoto, Z. Zhang, N. Sugiyama, Y. Honda, L. J. Schowalter, C. Sasaoka, and H. Amano, Appl. Phys. Express **14**, 051003 (2021).